Proton-Activated Chloride Channel Increases Endplate Porosity and Pain in a Mouse Spinal Degeneration Model

Peng Xue[1#], Weixin Zhang[1#], Mengxi Shen[1], Junhua Yang[3], Jiachen Chu[3], Shenyu Wang[1], Mei Wan[1,2], Junying Zheng[1], Zhaozhu Qiu[3,4*] and Xu Cao[1,2*]

[1]Center for Musculoskeletal Research, Department of Orthopedic Surgery, Johns Hopkins University School of Medicine, Baltimore, Maryland 21205, USA.

[2]Department of Biomedical Engineering, Johns Hopkins University School of Medicine, Baltimore, Maryland 21205, USA.

[3]Department of Physiology, Johns Hopkins University School of Medicine, Baltimore, MD 21205, USA.

[4]Solomon H. Snyder Department of Neuroscience, Johns Hopkins University School of Medicine, Baltimore, MD 21205, USA.

[#] Authors contributed equally.*Authors for correspondence:

Xu Cao, Ph.D., Center for Musculoskeletal Research, Department of Orthopedic Surgery, Johns Hopkins University School of Medicine, Ross Building, Room 209, 720 Rutland Avenue, Baltimore, MD 21205, USA. Phone number: 4105026440; E-mail: xcao11@jhmi.edu

Zhaozhu Qiu, Ph.D., Department of Physiology, Johns Hopkins University School of Medicine, WBSB Room 216, 725 N Wolfe St, Baltimore, MD 21205, USA. Phone number: 4106143795; E-mail: zhaozhu@jhmi.edu

Abstract

Chronic low back pain (LBP) can severely affect daily physical activity. Aberrant osteoclast-mediated resorption leads to porous endplates for the sensory innervation to cause LBP. Here, we report that the expression of proton-activated chloride (PAC) channel is induced during osteoclast differentiation in the porous endplates via a RANKL-NFATc1 signaling pathway. Extracellular acidosis evokes robust PAC currents in osteoclasts. An acidic environment of porous endplates and elevated PAC activation-enhanced osteoclast fusion provoke LBP. Further, we find that genetic knockout of PAC gene *Pacc1* significantly reduces endplate porosity and spinal pain in a mouse LBP model, but it does not affect bone development or homeostasis of bone mass in adult mice. Moreover, both osteoclast bone resorptive compartment environment and PAC traffic from the plasma membrane to endosomes to form an intracellular organelle Cl channel have low pH around 5.0. The low pH environment activates PAC channel to increase sialyltransferase *St3gal1* expression and sialylation of TLR2 in initiation of osteoclast fusion. Aberrant osteoclast-mediated resorption is also found in most skeletal disorders, including osteoarthritis, ankylosing spondylitis, rheumatoid arthritis, heterotopic ossification, enthesopathy. Thus, elevated *Pacc1* expression and PAC activity could be a potential therapeutic target for LBP and osteoclast-associated pain.

Introduction

Skeletal disorders including osteoarthritis and spine degeneration are often associated with pain. Pain is a major reason people seek medical attention. Chronic low back pain (LBP) profoundly affects quality of life and daily physical activity, especially in the elderly population, and thus it is a key risk factor for the development of future health decline(1-3). Most LBP is nonspecific with no apparent pathoanatomical cause(4). Therefore, to understand the source of LBP and its underlying mechanism is essential for its therapy. The cartilaginous endplate is composed of a thin layer of hyaline cartilage positioned between the vertebral endplate, the coronal surface of each vertebra, and the nucleus pulposus, which is the inner core of the vertebral disc that acts as the shock absorber for each spinal unit. Our previous studies have demonstrated that aberrant osteoclast-mediated resorption of calcified cartilaginous endplates during spine degeneration generates a porous structure, and osteoclasts in porous endplates secrete Netrin-1, that allows for sensory innervation of the spinal unit, thus leading to LBP(5-7). But it is still unclear how osteoclast activity becomes aberrant during spinal degeneration.

Pain in skeletal disorders is often associated with aberrant osteoclast resorption in a very low pH environments(8, 9). Our recent study reveals that proton-activated chloride (PAC) channel is newly identified proton-activated Cl^- channel to be encoded by *Pacc1* (also known as TMEM206) opened by acidic pH. The channel is responsive to pathological acidic pH in ischemic brain injury and acid-induced neuronal cell death in mice(10). PAC represents a completely new ion channel family which has no obvious sequence homology to other membrane proteins, but it is highly conserved in vertebrates(11). There are two transmembrane (TM) helices in PAC, like the acid-sensing ion channel (ASIC) and the epithelial sodium channel (ENaC)(12). PAC structure study showed that the protein exists in two states: namely, a high-pH resting closed state and a low-pH proton-bound non-conducting state. PAC channel undergoes striking conformational changes when the pH drops from 8 to 4, leading to an opening of the channel and the conduction of anions across cellular membranes, thereby inducing diseases associated with tissue acidosis (acid-induced cell death). Interestingly, PAC also localizes in intracellular organelles (endosomes and macropinosomes) and regulates their pH and volume homeostasis(13). The aberrant osteoclast bone remodeling in some of major bone diseases such as osteoarthritis, rheumatoid arthritis and low back pain are likely

associated with low pH, therefore we set out to investigate the function of the PAC channel in osteoclast differentiation and resorption for LBP.

Osteoclasts are formed from macrophages/monocytes that in response to NF-kappa B ligand (RANKL) signaling become committed to a tartrate-resistant acid phosphatase (TRAP)-positive osteoclast lineage(14-16). $TRAP^+$ mononuclear cells first attach to the bone surface and then undergo fusion to form multinucleated osteoclasts(17). Osteoclasts are polarized to form ruffle membranes with abundant ATPase proton pump activity at the side attached to the bone(18). Chloride channels such as CIC-7 are important in the cell membrane and intracellular organelles(19). In osteoclasts, CIC-7 is predominantly localized to the ruffled border, a specialized membrane domain crucial for acidifying the resorption lacuna. This acidification process supports ATPase proton pump activity, thereby enabling bone resorption. It also expressed at the membrane of lysosome/endosome(20). At both lysosome/endosome membrane and the ruffled border, CIC-7 functions on the ionic homeostasis, and maintain the pH(21, 22). The compartment between the ruffled membrane and the bone surface within the osteoclast sealing zone is acidified by secretion of protons, leading to the dissolvement of the bone matrix material(23, 24). Aberrant osteoclast-mediated bone resorption and the secretion of Netrin-1 are associated with many major skeletal disorders, including low back pain (LBP), osteoarthritis, heterotopic ossification and ankylosing spondylitis, among others(5, 25-29). PAC is activated at low pH environment with implication of bone diseases, and it is imperative to know its function in osteoclast differentiation and resorption in conjunction with CIC-7.

In this study, we investigated the potential role of PAC in osteoclast function of the porous endplates in spine degeneration-associated LBP. We found that PAC expressed on both cell membrane and cytoplasm of osteoclasts and its open conformation only occurs under conditions of acidic microenvironment. Knockout of *Pacc1* significantly reduced osteoclast fusion and endplate porosity, as well as relieved LBP in a mouse model of spine degeneration, but the genetic deletion did not have any effect on bone development or bone homeostasis in adult mice. Together, our results show that *Pacc1*-encoded Cl^- channel activity is induced during acidosis, leading to abhorrent osteoclast-mediated resorption to generate endplate porosity that leads to LBP. As depletion of PAC activity prevented the development of LBP during spinal degeneration with no negative effect on bone modeling or remodeling,

representing a potential therapeutic target for LBP.

Results

Knockout of *Pacc1* significantly reduces spinal pain and endplate porosity in a mouse model of spine degeneration

During spinal degeneration, osteoclast activity is stimulated, leading to porosity of the endplates, and Netrin-1 secreted by osteoclasts induces $CGRP^+$ nerve innervation and thus causes LBP. To examine the potential role of PAC in osteoclast-mediated resorption of the endplate and the generation of its porosity, we utilized mice with genetic deletion of *Pacc1*(10). We then surgically manipulated the *Pacc1*$^{-/-}$ mice and their wild-type (WT) littermates to generate a mouse model of lumbar spine instability (LSI) as a form of spinal degeneration. By pain behavior tests, we found that pressure tolerance was significantly lower in the WT LSI mice at 4- and 8-weeks post-LSI induction compared to sham-treated WT mice, whereas the degree of change in pressure tolerance in the *Pacc1*$^{-/-}$ LSI mice was significantly less than in the WT LSI mice but still lower than the sham-operated mutant mice (Figure 1A). These results suggest that *Pacc1*-encoded activity is associated with endplate porosity-induced LBP. Furthermore, by measuring the paw withdrawal frequency (PWF) in von Frey tests to evaluate mechanical pain hypersensitivity, we found that mechanical hyperalgesia was significantly lower at 4- and 8-weeks post-LSI surgery in *Pacc1*$^{-/-}$ LSI mice relative to their WT LSI littermates (Figure 1B). We also conducted a spontaneous activity behavior test. The distance traveled and active time per 24 hours were significantly greater in *Pacc1*$^{-/-}$ LSI mice relative to their WT LSI littermates (Figure 1, C and D).

Next, we examined the sclerosis endplates by μCT and found that endplate porosity was significantly lower in *Pacc1*$^{-/-}$ LSI mice relative to WT LSI mice 8 weeks post-LSI induction (Figure 1, E-G). By immunostaining for CGRP as a readout of innervation, we found that *Pacc1*$^{-/-}$ LSI mice showed less sensory nerve innervation in the porous endplates compared to WT LSI mice (Figure 1H). We then stained L4-L5 caudal endplates with Safranin O and Fast Green staining and found greater cartilage area and less porosity proportion in the endplate of the *Pacc1*$^{-/-}$ LSI mice relative to WT LSI mice at 8 weeks post-surgery (Figure 1, I and J). Strikingly, by TRAP staining we found that the number of large multinuclear osteoclast cells

were lower in the *Pacc1*$^{-/-}$ LSI mice relative to WT LSI mice at 8 weeks post-surgery (Figure 1, K and L), suggesting that *Pacc1* expression promotes aberrant osteoclast fusion and function. Together, these results indicate that PAC plays a role in pathological osteoclast bone resorption during the generation of endplate porosity and LBP during LSI.

We also examined whether PAC expression plays a physiological role in normal osteoclast bone resorption, bone development and bone remodeling. First, we investigated the effect of PAC on skeletal development and adult bone homeostasis. We examined the body length and weight at 1, 3 and 6 months of age, and we found that *Pacc1*$^{-/-}$ mice showed no difference with their WT littermates (Figure 2, A and B). Notably, we measured various bone parameters during development and adulthood by μCT at 1, 3 and 6 months of age. We found that important bone parameter bone volume in *Pacc1*$^{-/-}$ mice was not different than WT *Pacc1*$^{+/+}$ mice at 3 months of age (Figure 2, C and D). Furthermore, by TRAP staining of femur sections, we found that osteoclast numbers did not change in *Pacc1*$^{-/-}$ mice relative to WT *Pacc1*$^{+/+}$ mice at 3 months of age (Figure 2, E and F). Further, by osteocalcin staining, we found no difference in bone formation between *Pacc1*$^{-/-}$ and WT mice at 3 months of age (Figure 2, G and H). Taken together, these results indicate that PAC expression does not play a critical role in osteoclast bone resorption during bone development or in bone homeostasis under physiological conditions.

PAC expression is induced during osteoclast differentiation

To examine whether PAC expression is induced during osteoclast differentiation and resorption, whole-bone marrow cells were isolated from C57BL/6 mouse hind limbs and cultured with M-CSF (50 ng/mL) for 2 days to induce growth of bone marrow macrophages (BMMs). BMMs were then treated with M-CSF (30 ng/mL) and RANKL (100 ng/mL) for 5 days to induce osteoclast differentiation, as well as their fusion into mature osteoclasts (mOCs) (Figure 3A). *Pacc1* mRNA expression was significantly induced by RANKL stimulation relative to the M-CSF group at 1, 3 and 5 days and peaked at day 3 as measured by RT-PCR (Figure 3B). To confirm expression of the *Pacc1*-encoded channel protein during osteoclast differentiation, BMMs were treated with RANKL and harvested at day 0, 1, 3 and 5 for Western blot analysis of PAC expression. Consistent with the pattern of mRNA expression, PAC expression was higher in the RANKL-treated cells compared to the M-CSF-only treated cells with peak

expression at day 3 (Figure 3, C and D). We next examined the expression of NFATc1, a downstream transcription factor induced by RANKL signaling, and found that its expression was greater with treatment of RANKL in a time-dependent manner that matches that of PAC, suggesting that NFATc1 transcriptionally regulates *Pacc1* expression. We found three potential NFATc1-binding sites in the *Pacc1* promoter (Figure 3E), and by a chromatin immunoprecipitation (ChIP) assay we demonstrated that RANKL induced specific binding of NFATc1 to the most proximal NFATc1-binding site of the *Pacc1* promoter to activate its expression in osteoclast cells (Figure 3, F and G). Thus, PAC expression is induced during osteoclast maturation and bone resorption.

Extracellular acidosis evokes the robust PAC currents in osteoclasts

To examine the functional activity of PAC, BMMs were isolated from WT and *Pacc1*$^{-/-}$ mice and cultured with neutral (pH = 7.4) or acidic (pH = 6.8) medium containing M-CSF and RANKL. By RT-PCR and Western blot analysis, extracellular acidosis did not influence *Pacc1* or PAC expression at 1, 3 and 5 days of osteoclast differentiation (Figure 4, A-C). Furthermore, co-immunostaining of PAC with TRAP on human bone sections demonstrated that PAC was expressed on the cellular membrane and intracellular organelles of osteoclasts and well co-localized with TRAP staining at bone surface (Figure 4D). Indeed, by whole-cell patch clamping we found that extracellular acidosis evoked the proton-activated chloride currents in *Pacc1*^{wt} preosteoclasts at day 3 after RANKL treatment, while they were absent in *Pacc*1$^{-/-}$ cells (Figure 4, E and F). These results demonstrate that PAC is functionally expressed in osteoclast lineage cells and the channel is activated under acidic conditions. The results suggest that the function of PAC is not specific for osteoclast bone resorption like chloride transporter CIC-7, but likely in regulation of osteoclast fusion under low pH environment.

Knockout of *Pacc1* in TRAP^{+} cells reduce spinal pain and endplate porosity in the LSI model

To examine how PAC expression in osteoclast induces LBP, we crossed the floxed *Pacc1* mice (*Pacc1*$^{flox/flox}$) with TRAP-Cre to generate conditional *Pacc1*$_{TRAP}^{-/-}$ mice. We then conducted a series of pain behavior tests with the *Pacc1*$_{TRAP}^{-/-}$ mice and found that pressure tolerance was

significantly greater in *Pacc1*$_{TRAP}^{-/-}$ LSI mice relative to the *Pacc1*^{wt} LSI mice at both 4- and 8-weeks post operation (Figure 5A). Moreover, mechanical hyperalgesia, as measured by von Frey tests, was lower in *Pacc1*$_{TRAP}^{-/-}$ LSI mice at 4 and 8 weeks after operation compared to *Pacc1*^{wt} LSI mice (Figure 5B). In addition, distance traveled and active time per 24 hours spontaneous activity were significantly greater in *Pacc1*$_{TRAP}^{-/-}$ LSI mice relative to *Pacc1*^{wt} LSI mice at both 4- and 8-weeks post-surgery (Figure 5, C and D). As expected, by μCT scanning we found that there was less endplate porosity and Tb.Sp in *Pacc1*$_{TRAP}^{-/-}$ LSI mice relative to *Pacc1*^{wt} LSI mice at 8 weeks after surgery (Figure 5, E-G). And by immunostaining CGRP we found less sensory nerve innervation in the porous endplates in *Pacc1*$_{TRAP}^{-/-}$ LSI mice compared to *Pacc1*^{wt} LSI mice (Figure 5H). Therefore, PAC expression enhanced osteoclast resorptive activity to generate porous endplates, leading to pain hypersensitivity in a mouse model of spine degeneration.

PAC-mediated $I_{Cl,H}$ current activity in response to extracellular acidosis enhances osteoclast fusion

Next, we investigated PAC functional activity during osteoclast-mediated bone resorption. Osteoclasts prepared from either *Pacc1*$^{-/-}$ or *Pacc1*^{WT} mice were cultured on bone slices to examine their bone resorptive activity, which is referred to as a pit assay. The bone resorptive areas were significantly greater underneath osteoclastic cells from *Pacc1*^{WT} mice in pH 6.8 medium relative to pH 7.4 (Figure 6, A and B), an effect that was blunted among osteoclastic cells from *Pacc1*$^{-/-}$ mice in pH 6.8 medium, indicating that PAC expression enhances osteoclast reportion in a mildly low pH environment. We recorded a higher $I_{Cl,H}$ current on the membrane in TRAP^{+} mononuclear cells than in multinuclear cells at 3 days after RANKL treatment (Figure 6C). The PAC-mediated $I_{Cl,\,H}$ current of multinuclear cells was significantly lower at day 5 relative to day 3 after RANKL treatment (Figure 6D), indicating that PAC primarily regulates TRAP^{+} mononuclear cells prior to their osteoclast fusion. Moreover, by TRAP staining we found that extracellular acidosis accelerated osteoclast fusion in BMMs isolated from *Pacc1*$^{+/+}$ mice in pH 6.8 medium at day 3 and 5 after RANKL treatment (Figure 6, E and G, Supplemental Figure 1A). The results were further confirmed by phalloidin staining (Figure 6, F and H, Supplemental Figure 1A), which showed that osteoclast fusion in response to an

acidic medium was blunted in BMMs from *Pacc1*$^{-/-}$ mice. Taken together, our data indicate that PAC is required for osteoclast fusion at low pH.

PAC is essential for sialyltransferase *St3gal1* expression for osteoclast fusion by inducing sialylation of TLR2

We have reported that sialyltransferase St3gal1-mediated sialylation of TLR2 on preosteoclast initiates osteoclast fusion (30, 31). To investigate whether PAC regulates osteoclast fusion through the sialylation of TLR2, BMM isolated from *Pacc1*$^{+/+}$ and *Pacc1*$^{-/-}$ mice were treated with M-CSF and RANKL for three days at acidic and physiological pH conditions as we described before. The total protein was harvested for Western Blot analysis. We found that the expression of St3gal1 was minimum expressed at pH 7.4 but significantly increased at pH 6.8. Importantly, St3gal1 expression was significantly decreased in *Pacc1*$^{-/-}$ cells at both acidic and physiological pH medium (Figure 7, A and B) suggesting that activation of PAC at low pH promotes expression of St3gal1 to initiate preosteoclast fusion through St3gal1-mediated TLR2 sialylation. To examine PAC essential for *St3gal1* expression to initial osteoclast fusion, we knocked down *St3gal1* in *Pacc1*$^{+/+}$ or *Pacc1*$^{-/-}$ BMMs using siRNA against *St3gal1* (150809, Thermo Fisher), and the result showed the number of fused cells significantly decreased in *St3gal1* siRNA treated groups relative to control siRNA groups at different pH condition (Figure 7, C and D, Supplemental Figure 1, B-E). Osteoclast fusion marker, OC-STAMP, was also significantly decreased in the *St3gal1* knocked down groups at different pH environments (Supplemental Figure 1, F-I). Thus, under low pH microenvironment, *St3gal1* expression requires PAC activity to induce sialylation of TLR2 for osteoclast fusion.

Discussion

Endplates are cartilaginous structures connecting the vertebral body with the intervertebral disc in the spine. Endplates undergo porous sclerosis with partial ossification in patients with spine degeneration. Normally osteoclasts do not resorb cartilage, but they can target partially calcified cartilage in the porous endplates, in which the confined environment is marked by sensory innervation, angiogenic type H vessels and a low pH. Importantly, aberrant osteoclast resorption is found in many skeletal disorders with similar pathological environments including

osteoarthritis(25, 29), ankylosing spondylitis(26), rheumatoid arthritis(32, 33), enthesopathy(34), spine degeneration(5), heterotopic ossification(28), and Paget disease(35). The osteoclast-mediated resorptive activity in the pathological environment produces excessive Netrin-1, PDGF-BB, TGF-β and IGF-1 to promote the progression of skeletal disorders and pain(36-38). In our LSI animal model, the pH in the porous endplates we measured was 6.92 ± 0.08 (Supplementary Figure 2A). In addition, the Warburg effect is known as an important mechanism in generation of acidic microenvironment by elevated expression of lactic dehydrogenase A (LDHA)(39, 40). LDHA significantly accumulated in endplates of LSI mice (Supplementary Figure 2, B and C). Moreover, PAC expression is induced by NFATc1 with RANKL stimulation on the membrane and intracellular organelles of osteoclasts as RANKL induces the commitment of macrophages to the $TRAP^+$ osteoclast lineage for osteoclast fusion and maturation(30, 31). Interestingly, both the osteoclast bone resorptive compartment environment and PAC traffic from the plasma membrane to endosomes to form an intracellular organelle Cl channel have low pH around 5.0. The low pH environment activates PAC channel to increase *St3gal1* expression for sialylation TLR2 in initiation of osteoclast fusion.

Chloride channels/transporters such as CIC-7, coded by *Clcn7* gene, are important in the cell membrane and intracellular organelles(19). CIC-7 is primarily localized at the ruffled border of osteoclasts. Ruffled border is a special membrane area that important for the acidification and bone resorption. It also expressed at the membrane of lysosome/endosome(20). At both lysosome/endosome membrane and the ruffled border, CIC-7 contributes to the ionic homeostasis, and maintain the pH(21, 22). Importantly, CIC-7 provides the chloride conductance in endosome/lysosome, along with the proton pumping in the osteoclast ruffled membrane(19, 20, 22). Comparing with CIC-7 expression is polarized in the osteoclast ruffled membrane to provide the chloride conductance in endosome/lysosome, along with the proton pumping, the PAC is evenly distributed on the membrane of $TRAP^+$ mononuclear cells and osteoclasts with primary function for osteoclast fusion. PAC is activated at low pH to induce expression of *St3gal1* to sialylated TLR2 for fusion of $TRAP^+$ mononuclear cells (Figure 7, A and B). Knockout of *Pacc1* reduced osteoclast fusion in the endplate of LSI mice, whereas osteoclast fusion and bone resorption were not affected at normal bone. At low pH, *Pacc1*$^{-/-}$

preosteoclasts are difficult to fuse for the formation of osteoclasts fusion. Thus, one of the important functions of PAC is to maintain osteoclast fusion at low pH environment.

We demonstrated that acidic environment promoted *Pacc1*$^{+/+}$ osteoclasts fusion but not *Pacc1*$^{-/-}$ osteoclasts, while elevation of resorption was around 50% due to the "sudden stimulus" instead of continuous cultivation as Tim Arnett described. Tim Arnett et al. uncovered a significant impact of extracellular protons on the osteoclast bone resorption. This study represents the initial direct evidence that low pH enhances cell-mediated bone resorption(41). Furthermore, they found that rat osteoclasts may be more sensitive to stimulation by CO_2 acidosis than by HCO_3^- acidosis(42). His group investigated the effect of small shifts in extracellular pH on the resorptive activity of rat osteoclasts in vitro and found that very slight alterations in ambient hydrogen ion concentration can effectively "switch on" or "switch off" rat osteoclasts in vitro(43). His group also examined the effects of HCO_3^- and CO_2 acidosis on osteoclast-mediated Ca^{2+} release from 3-day cultures of neonatal mouse calvaria and found that addition of H^+ reduced pH from 7.12 to 7.03 and increased Ca^{2+} release 3.8-fold, and CO_2 acidosis was a less effective stimulator of Ca^{2+} release than HCO_3^- acidosis over a similar pH range(44).

TRAP could be expressed in other cell types, such as leukocytes. Based on our results, bone homeostasis remained unchanged in PAC global knockout mice. Furthermore, TRAP conditional knockout *Pacc1*$_{TRAP}^{-/-}$ mice displayed osteoclast functional outcomes similar to those in global knockout *Pacc*$^{-/-}$ mice. Thus, knocking out *Pacc1* in leukocytes or other cell types is unlikely to exert significant indirect effects on the function of PAC in osteoclast fusion. Attachment of $TRAP^+$ mononuclear preosteoclasts on the bone surface initiates fusion to form polarized multinucleated osteoclastic cells(45). The compartmentalized resorption environment is established by a circumferential attachment sealing zone(46). The plasma membrane within the sealing zone develops the ruffled border with abundant V-type H1-ATPase proton pump activity(47). Across this membrane the osteoclasts actively secrete HCl into the compartment to dissolve the bone matrix. First, the ATPase proton pump inserts H^+ into the resorption compartment and then chloride ions passively cross the membrane via chloride channel(22). These two steps of the proton pump and chloride channel forms HCl to acidify the resorption compartment and alkalinize the cytoplasm. At physiological condition of

bone remodeling, the basolateral bicarbonate chloride exchanger corrects the cytoplasmic alkalinization by compensating for cytoplasmic chloride loss(48, 49), while the PAC channel involved in chloride exchange on cell membrane as well. However, at low pH in the porous endplates, PAC is highly activated to promote chloride transport, which leads to aberrant osteoclast fusion and the development of LBP (Figure 7E). The aberrant osteoclast activity leads to the secretion of many factors, including Netrin-1 and PDGF-BB, to induce sensory innervation and angiogenesis in the porous endplates that ultimately leads to LBP and spine degeneration(5, 38). Knocking out *Pacc1* significantly reduced endplate porosity and LBP. Therefore, PAC expression and activation in osteoclasts could be a potential therapeutic target for LBP or joint arthritis pain.

Materials and methods

Sex as a biological variable

Our study exclusively examined male mice following our previous studies. It is unknown whether the findings are relevant for female mice.

Mice and in vivo treatment

Pacc1$^{flox/flox}$, *Pacc1*$^{-/-}$ and *Pacc1*$^{+/+}$ mice were generated as previously described(10). The TRAP-Cre mouse strain was obtained from Dr. J. J. Windle (Virginia Commonwealth University, Richmond, VA). Heterozygous TRAP-Cre mice were crossed with *Pacc1*$^{flox/flox}$ mice. The offspring were intercrossed to generate the following genotypes: WT, TRAP-Cre (mice expressing Cre recombinase driven by Trap promoter), *Pacc1*$^{flox/flox}$ (mice homozygous for the *Pacc1* flox allele, referred to herein as *Pacc1*^{wt}) and TRAP-Cre; *Pacc1*$^{flox/flox}$ (conditional deletion of *Pacc1* in TRAP lineage cells, referred to herein as *Pacc1*$_{TRAP}^{-/-}$). Genotypes were determined by polymerase chain reaction analyses of genomic DNA, which was extracted from mouse tails within the following primers:

WT/KO Genotyping for *Pacc1*: Forward: 5′- TCCTGTTTGGACTCGGAACT -3′,

Reverse: 5′- TGGTAGCTGTGCCTGATGTC -3′,

TMEM206_REV1: 5′- TCCTCACATAAGGGGCATG -3′;

TRAP-Cre: Forward: 5′-ATATCTCACGTACTGACGGTGGG-3′,

Reverse: 5′-CTGTTTCACTATCCAGG TTACGG-3′;

Pacc1 loxP allele: Forward: 5′- GAAGCCAGGCCATTCTTTTT -3′,

Reverse: 5′- GCTCAAGGAAACCACTGAGG -3′.

We performed LSI surgery in 2-month-old male mice, that were either WT, *Pacc1*$^{-/-}$, *Pacc1*^{wt} and *Pacc1*$^{flox/flox}$. Briefly, the mice were anesthetized with ketamine (100 mg/kg, intraperitoneally) and xylazine (10 mg/kg, intraperitoneally). Then, the LSI mouse model was created by resecting the L3–L5 spinous processes and the supraspinous and interspinous ligaments to induce instability of the lumbar spine (10–12 mice per group). Sham operations involved detachment of the posterior paravertebral muscles from L3–L5 only in a separate group of mice (10–12 mice per group)(50). All mice were maintained at the animal facility of The Johns Hopkins University School of Medicine.

Human subjects

Following approval from the Institutional Review Board (IRB; Johns Hopkins Institutional Review Boards), we procured human joint tissue samples. Our institutional IRB granted a waiver of consent for the participants, as the specimens comprised de-identified tissue archived by the pathology department. This approach aligns with the US Food and Drug Administration's regulations on consent waiver (Organization Policy FDA 50.1), permitting the use of such samples for research without individual consent due to the anonymity and pre-existing status of the tissue.

Behavioral testing

Behavioral testing was performed for *Pacc1*$^{-/-}$, *Pacc1*^{wt} mice with sham or LSI surgery. All behavioral tests were performed by the same blinded investigator in the study group Pressure thresholds were measure (SMALGO algometer, Bioseb) as pressure hyperalgesia(51). The L4-L5 spine was pressed by a 5-mm-diameter sensor tip while the mice were gently restrained. We gradually increased the pressure force at 50 g/s until an audible vocalization was heard. The pressure force was read by BIO-CIS software (Bioseb). A cutoff force was set as 500 g to prevent tissue trauma. The mice were allowed to rest for 15 min between tests, and the mean

value was calculated as the pressure tolerance threshold.

For the Von Frey test, we used Von Frey filament of 0.4 g (Stoelting) to test the frequency of hind paw withdrawal. Mice were placed on a wire metal mesh grid covered with a black plastic cage. Mice were set to acclimatize to the environment for at least 30 min before testing. The mid-plantar surface was stimulated by the filament for 2 seconds. The withdrawal frequency was recorded as the result of mechanical nociceptive threshold of the mice in response to 10 applications.

Spontaneous wheel-running activity was recorded using activity wheels designed for mice (model BIO-ACTIVW-M, Bioseb). The software enabled recording the activities of a mouse in the wheel cage. The mice were acclimatized to the environment for overnight before testing. And the test will be lasted for 48 hours for each mouse. The parameters of the spontaneous activities will be automatically recorded.

μCT

Mice were killed by isoflurane and perfused by 10% buffered formalin. For the analysis of endplates, the L3-L5 lumbar spine was collected and examined by μCT (voltage, 55 kVp; current, 181 μA; 9.0 μm per pixel) (Skyscan, 1172). For the analysis of femurs, the femur was collected and examined by μCT (voltage, 65 kVp; current, 153 μA; 9.0 μm per pixel) (Skyscan, 1172). Images were reconstructed by using NRecon v1.6 software (Skyscan). Quantitative analysis of the μCT results was performed by using CTAn v1.9 software (Skyscan). For the endplates, six consecutive images of the L4-L5 caudal endplates and L5 vertebrae (coronal view) were selected to show the 3-dimensional reconstruction results by using CTVol v2.0 software (Skyscan). For the femurs, we created cross-sectional images of the femur to perform three-dimensional analyses of trabecular bone by using CTVol v2.0 software (Skyscan).

Histochemistry, immunofluorescence, and histomorphometry for histological section

At the time of killing, the L3-L5 lumbar spine and femur samples were collected and fixed in 10% buffered formalin for 24 h. Both human and mouse bone samples were decalcified at 4°C using 0.5M ethylenediamine tetra acetic acid for two months or 3 weeks with constant shaking and then embedded in paraffin or 8% gelatin in the presence of 20% sucrose and 2%

polyvinylpyrrolidone. Four-μm-thick coronal-oriented sections of the L4–L5 lumbar spine were processed for Safranin O and fast green and TRAP (Sigma-Aldrich) staining using a standard protocol. Four-μm-thick sections of human tibia tissue were used for co-immunofluorescence staining of PAC and TRAP. Forty-μm-thick coronal-oriented sections were prepared for sensory nerve-related immunofluorescent staining, and 10-μm-thick coronal-oriented sections were used for other immunofluorescent staining using a standard protocol. The sections were incubated with primary antibodies to CGRP (1:100, ab81887, Abcam), PAC (1: 500, noncommercial antibody), TRAP (1:200, ab191406, Abcam) for 48 hours at 4 °C. Then, the corresponding secondary antibodies were added onto the sections for 1 h while avoiding light. The sections were then counterstained with 4′,6-diamidino-2-phenylindole (DAPI, Vector, H-1200). The sample images were observed and captured by a fluorescence microscope (Olympus BX51, DP71) or confocal microscope (Zeiss LSM 780). ImageJ (National Institutes of Health, Bethesda, MD) software was used for quantitative analysis.

Cell isolation and culture

The hind limbs of 8-week-old mice were harvested by carefully removing the attached soft tissue. We collected bone marrow cells by cutting both ends of the tibia and femur and then flushing the marrow with a syringe using α-minimum essential medium (α-MEM) (Sigma-Aldrich). Whole bone marrow cells were collected through centrifugation for 15 min at 1000 rpm and then cultured in α-MEM with 10% fetal bovine serum (FBS) (Sigma-Aldrich) at 37 °C in a 5% CO2-humidified incubator. After 24 h, the non-adherent cells floating in the culture media were collected and cultured in α-MEM with M-CSF (30 ng/ml). After 3 days, the macrophage-lineage cells were collected by digesting the adherent cells with Versene Solution (Thermo Fisher). The bone marrow macrophages (BMM) were reseeded in 6-well plates (5×10^5 cells per well), 24-well plates with cover slips (5×10^5 cells per well) or 96-well plates with bone slices (1×10^6 cells per well), and cultured in α-MEM containing 30 ng/ml M-CSF and 100 ng/ml RANKL (PeproTech). The pH level of cell culture medium was calibrated by blood gas analyzer at Johns Hopkins Medical Laboratory.

RT-PCR

The total RNA was extracted from the cells using TRIzol reagent (Invitrogen) according to the manufacturer's instructions. The purity of RNA was tested by measuring the ratio of absorbance at 260 nm over 280 nm. For RT-PCR, 1 μg RNA was reverse transcribed into complementary DNA using the SuperScript First-Strand Synthesis System (Invitrogen), then RT-PCR was performed with SYBR Green-Master Mix (Qiagen) on a C1000 Thermal Cycler (Bio-Rad Laboratories). Relative expression was calculated for each gene by the $2^{-\Delta\Delta}$ CT method, with glyceraldehyde 3-phosphate dehydrogenase for normalization. Primers used for RT-PCR are listed as below:

Pacc1: forward: 5′- ATGATCCGACAAGAACTCTCCA -3′,

reverse: 5′- AGCAGGACCGAGAAGACATTC -3′;

GAPDH: forward: 5′- AATGTGTCCGTCGTGGATCTGA -3′,

reverse: 5′- AGTGTAGCCCAAGATGCCCTTC -3′;

St3gal1: forward: 5′- CCACAACGCTCTGATGGAGG -3′,

Reverse: 5′- AACAGTTCCTTGACGGTGTCG -3′,

OC-STAMP: forward: 5′- CTGTAACGAACTACTGACCCAGC -3′,

Reverse: 5′- CCAGGCTTAGGAAGACGAAGA -3′.

Western blotting

The cell lysates were centrifuged and separated by 10% SDS-PAGE and transferred onto a polyvinylidene difluoride membrane (Bio-Rad Laboratories). After blocking with 5% BSA in Tris-buffered saline containing 0.05% Tween-20 (TBST), the membrane was incubated with specific primary antibodies at 4°C overnight. The membrane was then washed with TBST and incubated with horseradish peroxidase (HRP)-conjugated secondary antibodies. We detected protein using an enhanced chemiluminescence kit (Thermo Fisher Scientific). We used primary antibodies recognizing mouse PAC (1:500, Ab99055, Abcam), NFATc1 (1:500, MA3-024, Thermo Fisher), St3gal1 (1:1000, LS-C185763-100, Lifespan) β-actin (1:1000, 3700, cell signaling) and β-tubulin (1:1000, Ab108342, Abcam) to determine the protein concentrations in the lysates.

ChIP assay

We added cells with formaldehyde to cross-link proteins to DNA, and the cells were lysed in 1.5 mL lysis buffer (50 mM HEPES, pH 7.5, 140 mM NaCl; 1 mM EDTA; 1% Triton X-100; 0.1% sodium deoxy cholate; 0.1% sodium dodecyl sulfate). Cell lysates were sonicated at 2s on/15s off for three rounds using a Bioruptor ultrasonic cell disruptor (Diagenode) to shear genomic DNA to a mean fragment size of 150–250 bp. Of the sample, 1% was removed for use as input control. ChIP was performed according to the protocol provided by the Simple Chip Enzymatic Chromatin IP Kit (Cell Signaling Technology) using antibodies to NFATc1 (Thermo Fisher). Anti-RNA polymerase II and control IgG were used as positive and negative controls, respectively. After washing and de-crosslinking, the precipitated DNA was purified using a QIA quick PCR purification kit (Qiagen). The PCR primers used to detect NFATc1 binding site were as follows:

Site #1: Forward: 5′- ACTTGCTTTCCTGCTCCT -3′,

Reverse: 5′- TTCCCTGTCTATCTTCTTTCTA -3′;

Site #2, Forward: 5′- GCTAACCTGGACGCTTGT -3′,

Reverse: 5′- TTTGTTTGTGCTTGCTCT -3′;

Site #3, Forward: 5′- GGCTGATATTGGTTTGTA -3′,

Reverse: 5′- GTCCCTTCTTGTTTGTCT -3′.

Whole-cell electrophysiology

For whole-cell patch clamp recordings on the proton-activated Cl^- channel, the extracellular solution contains (in mM) 145 NaCl, 2 KCl, 2 $MgCl_2$, 1.5 $CaCl_2$, 10 HEPES, 10 glucose (300 mOsm/kg; pH 7.3 with NaOH). Different acidic pH solutions were made of the same ionic composition without HEPES but with 5 mM Na3-citrate as buffer and the pH was adjusted using citric acid. Patch pipettes were fabricated from borosilicate glass (Sutter Instruments) and pulled with a Model P-1000 multi-step puller (Sutter Instruments) and had a resistance of 2-4 MΩ when filled with an internal solution containing (in mM): 135 CsCl, 1 $MgCl_2$, 2 $CaCl_2$, 10 HEPES, 5 EGTA, 4 MgATP (280-290 mOsm/kg; pH 7.2 with CsOH). Extracellular solutions were applied using a gravity perfusion system with a small tip about 100-200 μm away from the recording cell. All experiments were done at 37-degree. Recordings were made with MultiClamp 700B amplifier and 1550B digitizer (Molecular Devices). Signals were filtered at 2 kHz and digitized at 10 kHz. The capacitive transients were compensated just

before each measurement and the series resistance then was routinely compensated for at least 80%.

For PAC current recording, cells were held at 0 mV and voltage ramps (500 ms duration) were applied from -100 to +100 mV. Data was analyzed using Clampfit 10.6 and GraphPad Prism 6.

Bone resorption assay

To assess the effect of PAC-induced bone resorption in acidic condition, we performed an osteoclast bone resorption assay using a commercially available bone resorption assay kit (Cosmo Bio). Briefly, BMM isolated from *Pacc1*$^{-/-}$ and *Pacc1*$^{+/+}$ mice were seeded on bone slices in 24-well plates and cultured in acidic or neutral osteoclastogenic medium for 7 days. The resorption pits on the hydroxyapatite surface were imaged under a microscope.

Staining of the osteoclasts

Cells were cultured in osteoclastogenic medium for 1, 3 or 5 days, and fixed for 10 minutes by using 4% paraformaldehyde. A TRAP staining kit (Sigma-Aldrich) was used to detect TRAP^{+} cells according to the manufacturer's instructions. We used fluorescence staining of F-actin with phalloidin to observe action ring formation. Sample images were captured by a fluorescence microscope (Olympus BX51, DP71).

siRNA interference

For in vitro siRNA interference, mouse *St3gal1* siRNA (150809, Thermo Fisher) and control siRNA (4390843, Thermo Fisher) were transfected into primary *Pacc1*$^{+/+}$ and *Pacc1*$^{-/-}$ cells, using Lipofectamine RNAiMAX transfection kit (13778030, Thermo Fisher) and Opti-MEM Reduced Serum Medium (31985062, Thermo Fisher Scientific) according to the guideline from manufacture.

Endplate pH measurement

To conclusively determine the presence of acidic conditions in the spinal endplate area, we employed a Micro combination pH electrode with a needle tip for accurate in vivo pH assessments (9863BN Micro pH Electrode, Thermo Fisher). Both LSI and sham-operated mice

were sedated through intraperitoneal injections of ketamine (100 mg/kg) and xylazine (10 mg/kg). We then surgically exposed the L3-L5 endplates. To protect the surrounding tissues and precisely target the area of interest, sterile gauze was applied. For each mouse, we calculated the average pH values at the L3, L4, and L5 endplates, ensuring accurate representation of the local pH environment within the spinal endplate region.

Statistical analysis

All data analyses were performed using SPSS, version 24.0, software (IBM Corp). Data are presented as means ± standard deviations. In general, independent sample t-test was used for comparisons among two groups; and one-way ANOVA with Bonferroni's post hoc test was used for comparisons among multiple groups. For in vivo studies, two-way repeated ANOVA with Bonferroni post hoc test was performed to test the effect of LSI surgery or genotype on behavior test results at different time points. The effects of LSI surgery or genotype on endplate porosity, osteoclast function and gene expression were analyzed by two-way ANOVA with Bonferroni's post hoc test. For in vitro studies, two-way ANOVA with Bonferroni post hoc test was performed to test the effect of acidic condition or genotype on osteoclast differentiation and function. For all experiments, $p < 0.05$ was considered significant. All inclusion/exclusion criteria were preestablished, and no samples or animals were excluded from the analysis. No statistical method was used to predetermine the sample size. The experiments were randomized, and the investigators were blinded to allocation during experiments and outcome assessment.

Author Contributions

X. C., Z. Q., P. X. and W.Z. conceived of the study. P. X., S. W., J. C. and M. W. designed and conducted primary experiments. X. C. and P. X. wrote the manuscript. X. C., W. Z. and J.Z. contributed to craft the rebuttal and revise the manuscript, W.Z. and J.Y. contributed to the experiments for the revision, M.S. help with experiments. Mouse anti-Human PAC monoclonal antibody was provided by Z. Q.

Acknowledgments

This research was supported by NIH National Institute on Aging under Award Number

R01RF1AG068997 and P01AG066603 (to X.C.).

Competing Interests

No completing interests.

References

1. Tsuji S, et al. Low back pain is closely associated with frailty but not with sarcopenia: Cross-sectional study of rural Japanese community-dwelling older adults. *Geriatr Gerontol Int*. 2021;21(1):54-59.
2. Hawker GA. The assessment of musculoskeletal pain. *Clin Exp Rheumatol*. 2017;35 Suppl 107(5):8-12.
3. Tinnirello A, Mazzoleni S, Santi C. Chronic Pain in the Elderly: Mechanisms and Distinctive Features. *Biomolecules*. 2021;11(8):1256.
4. Wimalasundera N, Stevenson VL. Cerebral palsy. *Pract Neurol*. 2016;16(3):184-194.
5. Ni S, et al. Sensory innervation in porous endplates by Netrin-1 from osteoclasts mediates PGE2-induced spinal hypersensitivity in mice. *Nat Commun*. 2019;10(1):5643.
6. Xue P, et al. PGE2/EP4 skeleton interoception activity reduces vertebral endplate porosity and spinal pain with low-dose celecoxib. *Bone Res*. 2021;9(1):36.
7. Lv X, Gao F, Cao X. Skeletal interoception in bone homeostasis and pain. *Cell Metab*. 2022;34(12):1914-1931.
8. Nagae M, Hiraga T, Yoneda T. Acidic microenvironment created by osteoclasts causes bone pain associated with tumor colonization. *J Bone Miner Metab*. 2007;25(2):99-104.
9. Nagae M, Hiraga T, Wakabayashi H, Wang L, Iwata K, Yoneda T. Osteoclasts play a part in pain due to the inflammation adjacent to bone. *Bone*. 2006;39(5):1107-1115.
10. Yang J, et al. PAC, an evolutionarily conserved membrane protein, is a proton-activated chloride channel. *Science*. 2019;364(6438):395-399.
11. Capurro V, Gianotti A, Caci E, Ravazzolo R, Galietta LJ, Zegarra-Moran O. Functional analysis of acid-activated Cl^- channels: properties and mechanisms of regulation. *Biochim Biophys Acta*. 2015;1848(1 Pt A):105-114.
12. Ruan Z, Osei-Owusu J, Du J, Qiu Z, Lü W. Structures and pH-sensing mechanism of the proton-activated chloride channel. *Nature*. 2020;588(7837):350-354.
13. Osei-Owusu J, Yang J, Leung KH, Ruan Z, Lü W, Krishnan Y, et al. Proton-activated chloride channel PAC regulates endosomal acidification and transferrin receptor-mediated endocytosis. *Cell Rep*. 2021;34(4):108683.
14. Teitelbaum SL. Glucocorticoids and the osteoclast. *Clin Exp Rheumatol*. 2015;33(4 Suppl 92):S37-39.
15. Feng X, Teitelbaum SL. Osteoclasts: New Insights. *Bone Res*. 2013;1(1):11-26.
16. Feng X, and Teitelbaum SL. Osteoclasts: New Insights. *Bone Res*. 2013;1(1):11-26.
17. Novack DV, Faccio R. Osteoclast motility: putting the brakes on bone resorption. *Ageing Res Rev*. 2011;10(1):54-61.

18. Mattsson JP, Skyman C, Palokangas H, Väänänen KH, Keeling DJ. Characterization and cellular distribution of the osteoclast ruffled membrane vacuolar H+-ATPase B-subunit using isoform-specific antibodies. *J Bone Miner Res*. 1997;12(5):753-760.
19. Kornak U, Kasper D, Bösl MR, Kaiser E, Schweizer M, Schulz A, et al. Loss of the ClC-7 chloride channel leads to osteopetrosis in mice and man. *Cell*. 2001;104(2):205-15.
20. Kasper D, Planells-Cases R, Fuhrmann JC, Scheel O, Zeitz O, Ruether K, et al. Loss of the chloride channel ClC-7 leads to lysosomal storage disease and neurodegeneration. *EMBO J*. 2005;24(5):1079-91.
21. Nicoli ER, Weston MR, Hackbarth M, Becerril A, Larson A, Zein WM, et al. Lysosomal Storage and Albinism Due to Effects of a De Novo CLCN7 Variant on Lysosomal Acidification. *Am J Hum Genet*. 2019;104(6):1127-38.
22. Ribet A, Ng PY, Pavlos NJ. Membrane Transport Proteins in Osteoclasts: The Ins and Outs. *Front Cell Dev Biol*. 2021;9:644986.
23. Minoshima M, et al. In Vivo Multicolor Imaging with Fluorescent Probes Revealed the Dynamics and Function of Osteoclast Proton Pumps. *ACS Cent Sci*. 2019;5(6):1059-1066.
24. Teitelbaum SL. Bone resorption by osteoclasts. *Science*. 2000;289(5484):1504-8.
25. Zhu S, et al. Subchondral bone osteoclasts induce sensory innervation and osteoarthritis pain. *J Clin Invest*. 2019;129(3):1076-1093.
26. Yu T, et al. Chondrogenesis mediates progression of ankylosing spondylitis through heterotopic ossification. *Bone Res*. 2021;9(1):19.
27. Jin W, et al. Engineered osteoclasts as living treatment materials for heterotopic ossification therapy. *Nat Commun*. 2021;12(1):6327.
28. Wang X, et al. Inhibition of overactive TGF-β attenuates progression of heterotopic ossification in mice. *Nat Commun*. 2018;9(1):551.
29. Su W, et al. Senescent preosteoclast secretome promotes metabolic syndrome associated osteoarthritis through cyclooxygenase 2. *Elife*. 2022;11:e79773.
30. Dou C, Zhen G, Dan Y, Wan M, Limjunyawong N, Cao X. Sialylation of TLR2 initiates osteoclast fusion. *Bone Res*. 2022;10(1):24.
31. Zhang W, et al. RANK(+)TLR2(+) myeloid subpopulation converts autoimmune to joint destruction in rheumatoid arthritis. *Elife*. 2023;12:e85553.
32. Xu X, et al. Aberrant Activation of TGF-β in Subchondral Bone at the Onset of Rheumatoid Arthritis Joint Destruction. *J Bone Miner Res*. 2015;30(11):2033-2043.
33. Schett G, Teitelbaum SL. Osteoclasts and arthritis. *J Bone Miner Res*. 2009;24(7):1142-1146.
34. Wang X, et al. Aberrant TGF-β activation in bone tendon insertion induces enthesopathy-like disease. *J Clin Invest*. 2018;128(2):846-860.
35. Rabjohns EM, Hurst K, Ghosh A, Cuellar MC, Rampersad RR, Tarrant TK. Paget's Disease of Bone: Osteoimmunology and Osteoclast Pathology. *Curr Allergy Asthma Rep*. 2021;21(4):23.
36. Cui Z, et al. Halofuginone attenuates osteoarthritis by inhibition of TGF-β activity and H-type vessel formation in subchondral bone. *Ann Rheum Dis*. 2016;75(9):1714-1721.
37. Chen X, Wang Z, Duan N, Zhu G, Schwarz EM, Xie C. Osteoblast-osteoclast

interactions. *Connect Tissue Res*. 2018;59(2):99-107.
38. Xie H, et al. PDGF-BB secreted by preosteoclasts induces angiogenesis during coupling with osteogenesis. *Nat Med*. 2014;20(11):1270-1278.
39. Urata K, Kajihara I, Miyauchi H, Mijiddorj T, Otsuka-Maeda S, Sakamoto R, et al. The Warburg effect and tumour immune microenvironment in extramammary Paget's disease: overexpression of lactate dehydrogenase A correlates with immune resistance. *J Eur Acad Dermatol Venereol*. 2020;34(8):1715-21.
40. Yoneda T, Hiasa M, and Okui T. Crosstalk Between Sensory Nerves and Cancer in Bone. *Curr Osteoporos Rep*. 2018;16(6):648-56.
41. Arnett TR, and Dempster DW. Effect of pH on bone resorption by rat osteoclasts in vitro. *Endocrinology*. 1986;119(1):119-24.
42. Arnett TR, Boyde A, Jones SJ, and Taylor ML. Effects of medium acidification by alteration of carbon dioxide or bicarbonate concentrations on the resorptive activity of rat osteoclasts. *J Bone Miner Res*. 1994;9(3):375-9.
43. Arnett TR, and Spowage M. Modulation of the resorptive activity of rat osteoclasts by small changes in extracellular pH near the physiological range. *Bone*. 1996;18(3):277-9.
44. Meghji S, Morrison MS, Henderson B, and Arnett TR. pH dependence of bone resorption: mouse calvarial osteoclasts are activated by acidosis. *Am J Physiol Endocrinol Metab*. 2001;280(1):E112-9.
45. Søe K, Hobolt-Pedersen AS, Delaisse JM. The elementary fusion modalities of osteoclasts. *Bone*. 2015;73:181-189.
46. Takito J, Inoue S, Nakamura M. The Sealing Zone in Osteoclasts: A Self-Organized Structure on the Bone. *Int J Mol Sci*. 2018;19(4):984.
47. Blair HC, Teitelbaum SL, Tan HL, Koziol CM, Schlesinger PH. Passive chloride permeability charge coupled to H(+)-ATPase of avian osteoclast ruffled membrane. *Am J Physiol*. 1991;260(6 Pt 1):C1315-1324.
48. Edwards JC, Cohen C, Xu W, Schlesinger PH. c-Src control of chloride channel support for osteoclast HCl transport and bone resorption. *J Biol Chem*. 2006;281(38):28011-28022.
49. Schlesinger PH, Blair HC, Teitelbaum SL, Edwards JC. Characterization of the osteoclast ruffled border chloride channel and its role in bone resorption. *J Biol Chem*. 1997;272(30):18636-18643.
50. Ono K, Yonenobu K, Miyamoto S, Okada K. Pathology of ossification of the posterior longitudinal ligament and ligamentum flavum. *Clin Orthop Relat Res*. 1999;(359):18-26.
51. Kim JS, et al. The rat intervertebral disk degeneration pain model: relationships between biological and structural alterations and pain. *Arthritis Res Ther*. 2011;13(5):R165.

Figures and Legends

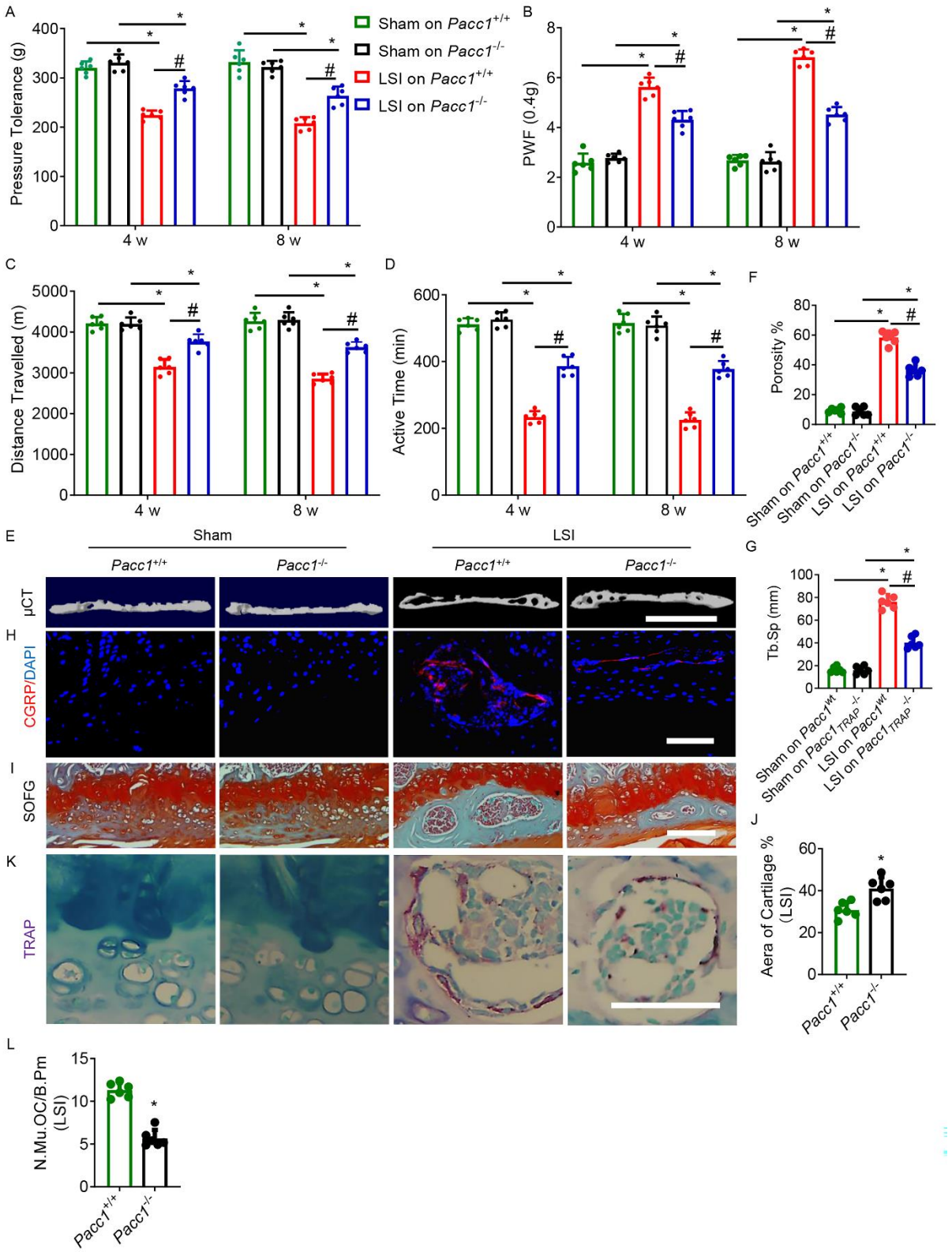

Figure 1. Knockout of *Pacc1* significantly reduces spinal pain and endplate porosity in a mouse model of spine degeneration.

(A) Pressure tolerance of the lumbar spine as assessed by the force threshold needed to induce

vocalization by a force gauge at 4 and 8 weeks after LSI surgery. (B) The hind paw withdrawal frequency in response to mechanical stimulation (von Frey, 0.4 g) a 4 and 8 weeks after LSI surgery. (C, D) Spontaneous activity analysis, including distance traveled (C) and active time (D) on the wheel per 24 h. (E) Representative 3-dimensional, high-resolution μCT images of the L4-L5 caudal endplates (coronal view) at 8 weeks after LSI surgery. Scale bars, 1 mm. n=6 per group. (F, G) Quantitative analysis of the total porosity (F) and trabecular separation (G) of the L4-L5 caudal endplates as determined by μCT. (H) Representative images of immunofluorescent analysis of CGRP (red) and DAPI (blue) staining of nerve fibers in the endplates at 8 weeks after LSI surgery. Scale bars, 50μm. (I) Representative images of Safranin O and fast green staining of coronal L4-L5 caudal endplate sections at 8 weeks after LSI surgery. Scale bars, 50μm. (J) Quantitative analysis of the area of cartilage in the endplate of *Pacc1*$^{+/+}$ and *Pacc1*$^{-/-}$ mice at 8 weeks after LSI surgery. (K) Representative images of coronal L4-L5 caudal endplate sections stained for TRAP at 8 weeks after LSI surgery. Scale bars, 50μm. (L) Quantitative analysis of the number of TRAP^{+} multinuclear cells in endplates.

(A-D, F, G) *$p < 0.05$ compared with sham group; and #$p < 0.05$ compared with *Pacc1*$^{+/+}$ mice after LSI surgery. n=6 per group. (J, L) *$p < 0.05$ compared with *Pacc1*$^{+/+}$ group. n=6 per group.

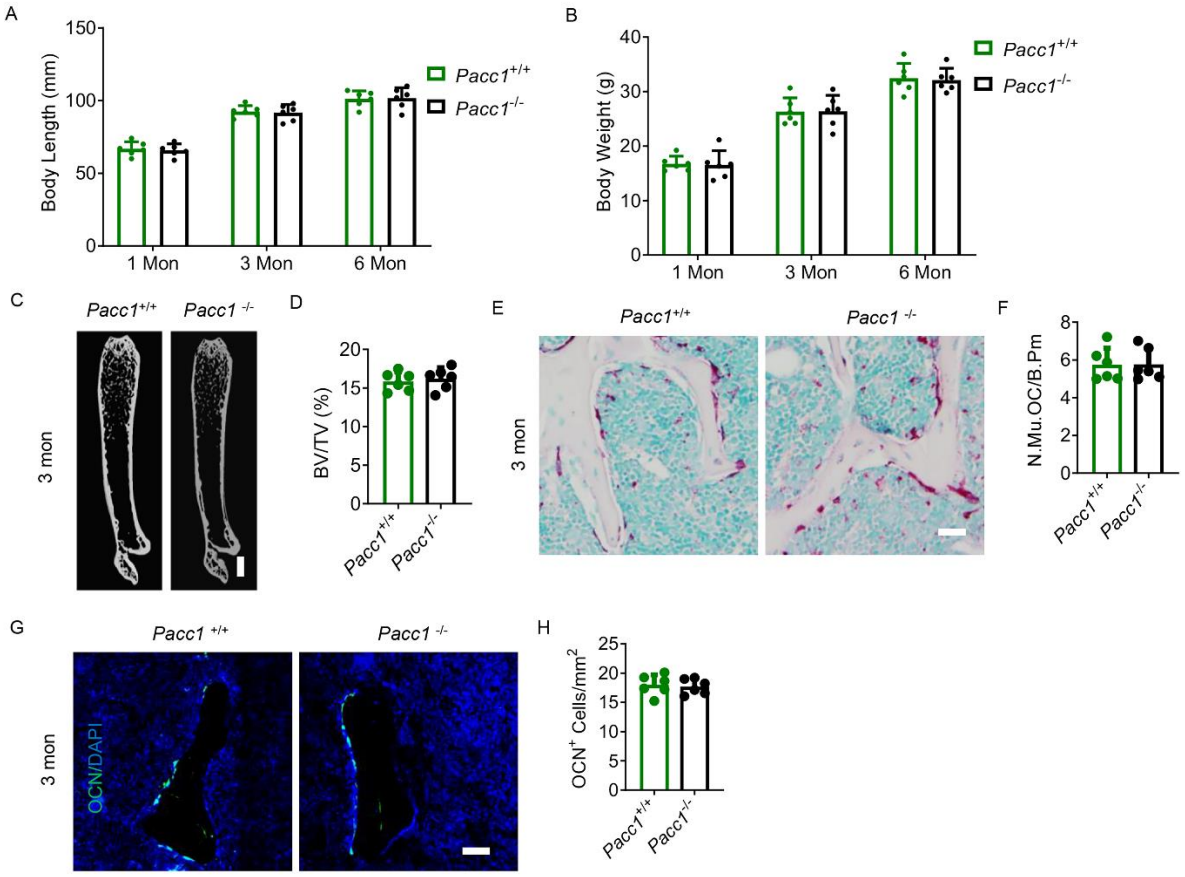

Figure 2. Knockout of *Pacc1* channel does not influence bone development or femur bone mass in adult mice.

(A) Body length of *Pacc1*$^{+/+}$ and *Pacc1*$^{-/-}$ mice, n ⩾ 5. (B) Body weight of *Pacc1*$^{+/+}$ and *Pacc1*$^{-/-}$ mice, n ⩾ 5. (C) Representative μCT images of femurs from 3-month-old male *Pacc1*$^{+/+}$ and *Pacc1*$^{-/-}$ mice. Scale bar: 1 mm. (D) Quantitative analysis of μCT result of femurs from 3-month-old male *Pacc1*$^{+/+}$ and *Pacc1*$^{-/-}$ mice, n = 6.(E) Representative images of TRAP staining for coronal femur sections from 3-month-old male *Pacc1*$^{+/+}$ and *Pacc1*$^{-/-}$ mice. Scale bars, 50μm. (F) Quantitative analysis of the number of TRAP^{+} multinuclear cells in femurs, n = 6.(G) Representative images of immunofluorescent analysis of osteocalcin (OCN) staining and DAPI (blue) staining of nuclei for coronal femur sections from 3-month-old male *Pacc1*$^{+/+}$ and *Pacc1*$^{-/-}$ mice. Scale bars, 50μm. (H) Quantitative analysis of the number of OCN^{+} cells in femurs, n = 6.

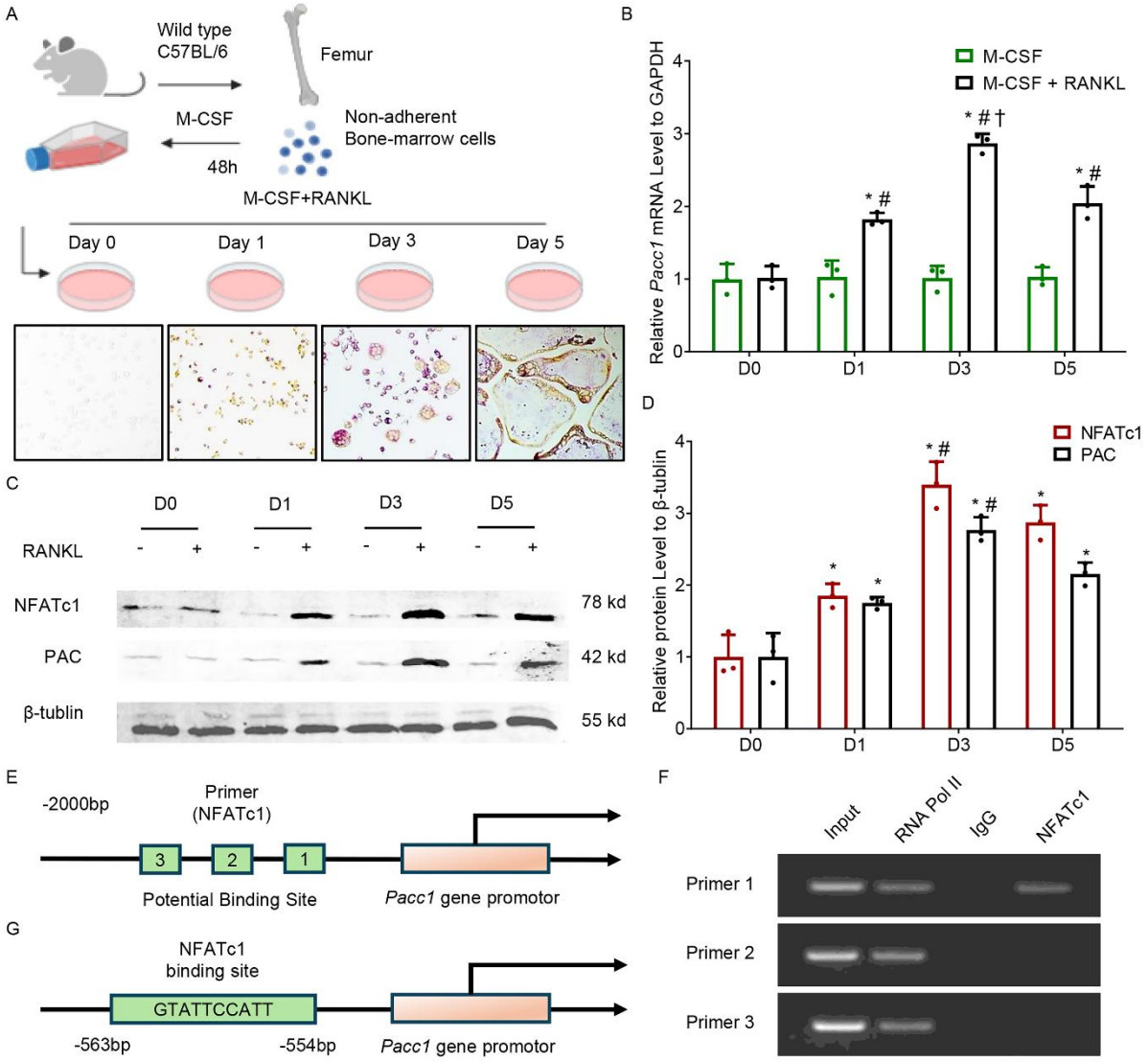

Figure 3. PAC expression is induced during osteoclast differentiation.

(A) A schematic diagram illustrating the preparation of $TRAP^+$ osteoclast precursors and their maturation process. (B) Relative mRNA expression levels of *Pacc1* in the cells cultured in the medium with or without RANKL at 0, 1, 3 and 5 days, n = 3. (C, D) Protein levels of NFATc1 and PAC at 0, 1, 3 and 5 days were analyzed by western blotting, n = 3. (E) Diagram of potential NFATc1 binding sites on the *Pacc1* promoter in osteoclast precursors. (F) ChIP analysis of NFATc1 on the *Pacc1* promoter. (G) Diagram of the *Pacc1* promoter with an NFATc1 binding site.

(B) *$p < 0.05$ compared with Day 0; #$p < 0.05$ compared with M-CSF group (without RANKL); and †$p < 0.05$ compared with Day 1. (D) *$p < 0.05$ compared with Day 0; and #$p < 0.05$ compared with Day 1.

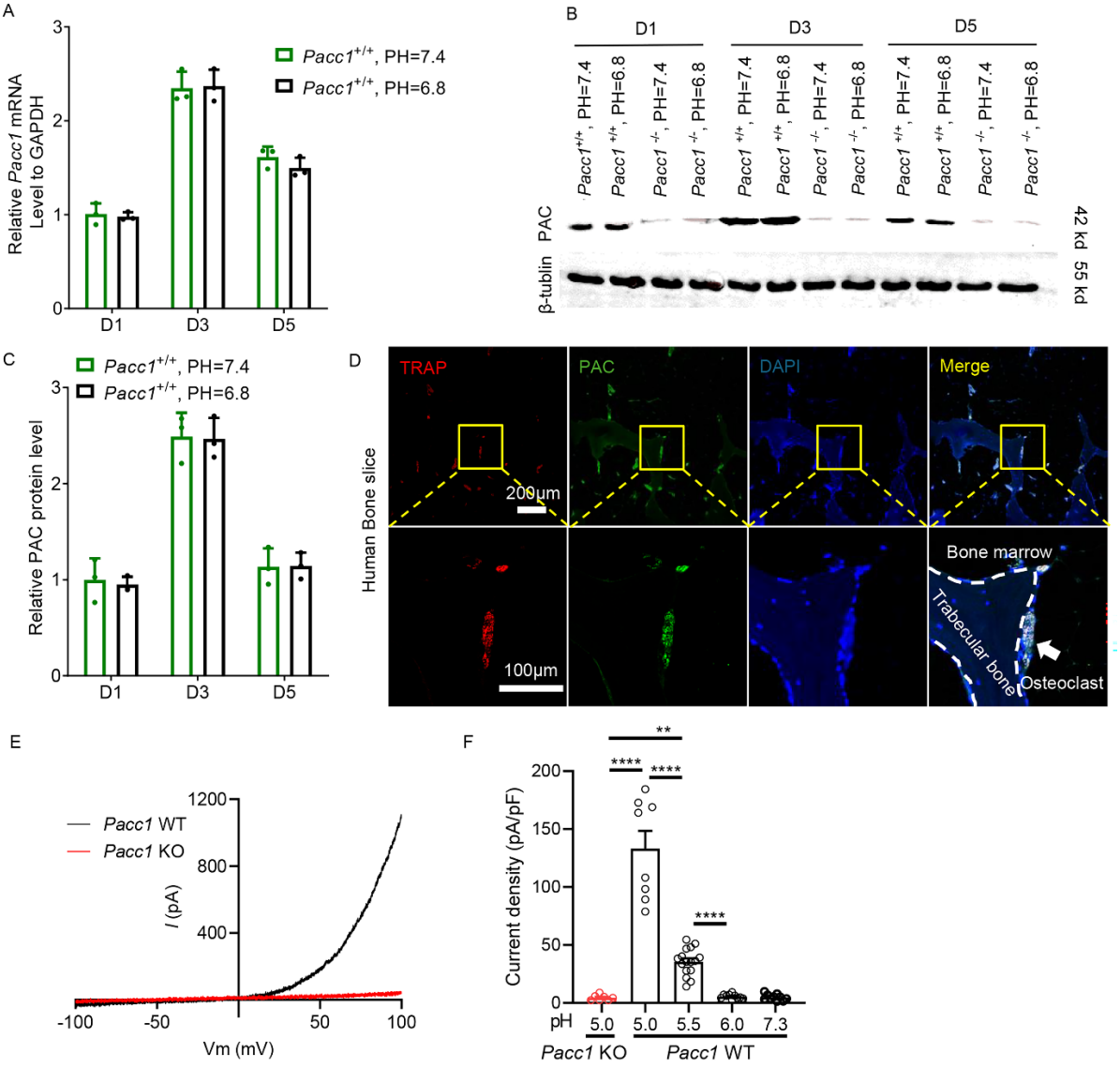

Figure 4. Extracellular acidosis evokes the $I_{Cl,\ H}$ current in the cell membrane of osteoclasts by activating PAC.

(A) Relative mRNA expression levels of *Pacc1* in the cells isolated from *Pacc1*$^{+/+}$mice cultured in neutral or acidic medium at 1, 3 and 5 day, n = 3s. (B, C) Protein levels of PAC in the cells isolated from *Pacc1*$^{+/+}$ or *Pacc1*$^{-/-}$ mice cultured in neural or acidic medium at 1, 3 and 5 days, n = 3. (D) The representative images of co-immunofluorescence staining of PAC (Green) and TRAP (Red) in human bone section. Scale bar: 200μm, 100μm. Blue: DAPI. (E) PAC currents monitored by voltage-ramp protocol at pH 5.5 in the cells isolated from *Pacc1*$^{+/+}$ or *Pacc1*$^{-/-}$ mice cultured in osteoclastic medium for 3 days. (F) PAC-mediated current densities measured at +100 mV in the cells isolated from *Pacc1*$^{-/-}$ (red) and *Pacc1*$^{+/+}$ (black) mice

cultured in osteoclastic medium for 3 days, at 5.0, 5.5, 6.0 and 7.3 at 37-degree temperature, n ⩾ 7.(E, F) *$p < 0.05$ compared with the cells isolated from *Pacc1*$^{+/+}$ mice. ** $p < 0.01$, ****$p < 0.001$.

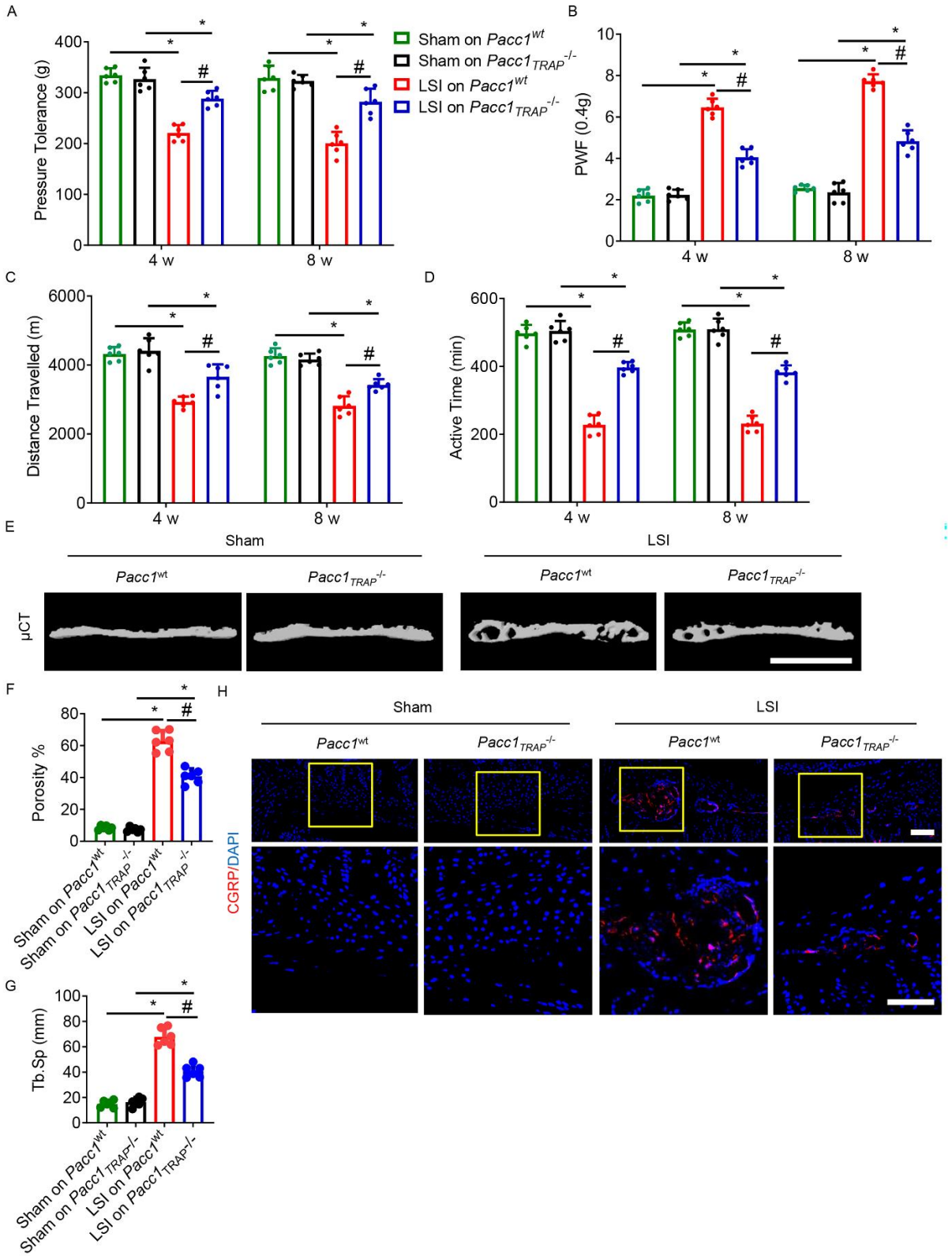

Figure 5. Knockout of PAC channel in TRAP^{+} cells reduce spinal pain and endplate porosity in the LSI model.

(A) Pressure tolerance of the lumbar spine as assessed by the force threshold needed to induce vocalization by a force gauge at 4 and 8 weeks after LSI surgery. (B) The hind paw withdrawal frequency in response to mechanical stimulation (Von Frey, 0.4 g) a 4 and 8 weeks after LSI surgery. (C, D) Spontaneous activity analysis, including distance traveled (C) and active time (D) on the wheel per 24 h. (E) Representative 3-dimensional, high-resolution μCT images of the L4-L5 caudal endplates (coronal view) at 8 weeks after LSI surgery. Scale bars, 1 mm. (F, G) Quantitative analysis of the total porosity (F) and trabecular separation (G) of the L4-L5 caudal endplates as determined by μCT. (H) Representative images of immunofluorescent analysis of CGRP (red) and DAPI (blue) staining of nerve fibers in the endplates at 8 weeks after LSI surgery. Scale bars, 50μm.

(A-D, F, G) *$p < 0.05$ compared with sham group; and #$p < 0.05$ compared with *Pacc1*^{wt} mice after LSI surgery. n=6 per group.

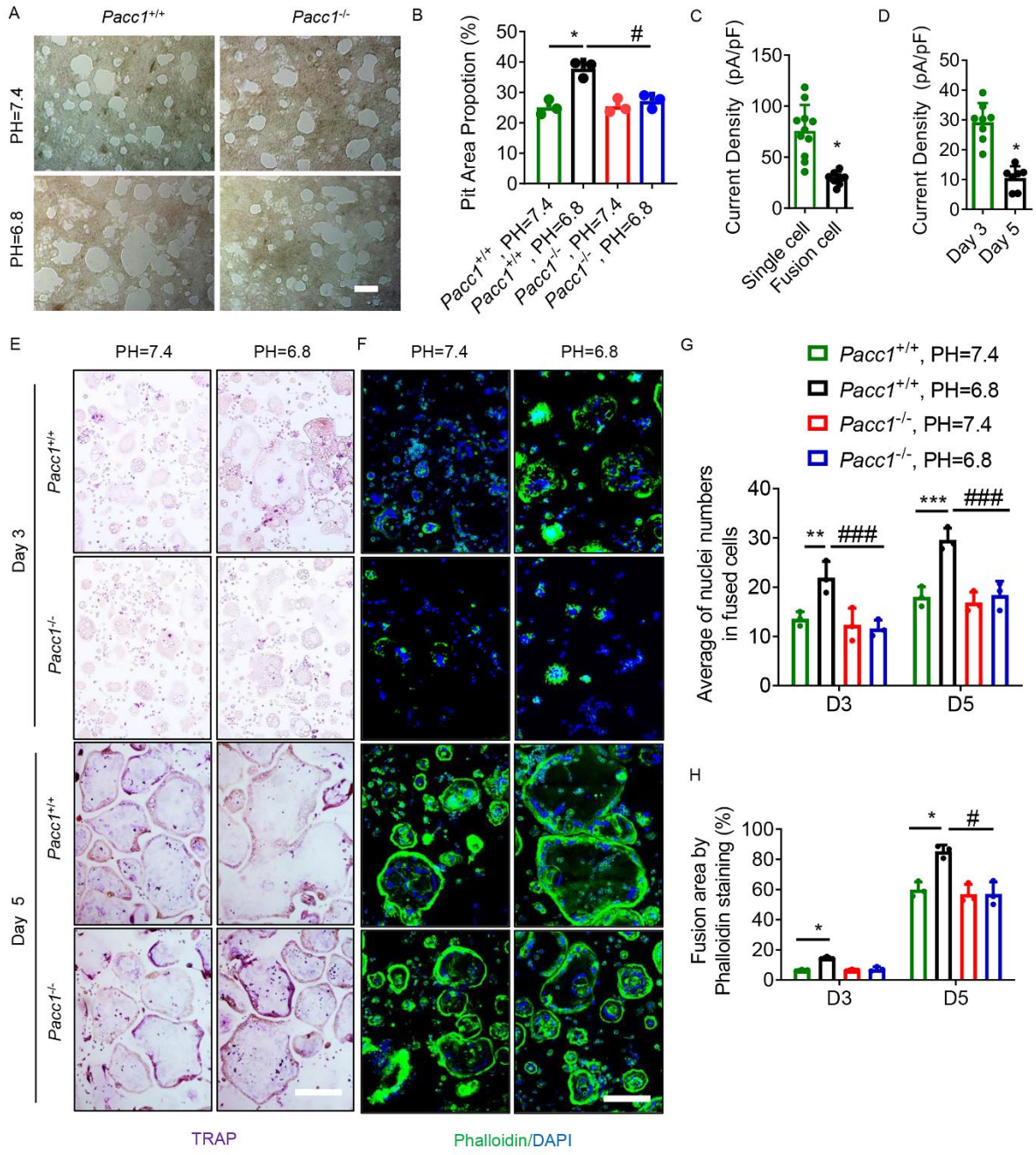

Figure 6. PAC-mediated $I_{Cl,\ H}$ current activity in response to extracellular acidosis enhances osteoclast fusion and resorption.

(A, B) Resorption pits of the cells isolated from *Pacc1*$^{+/+}$ or *Pacc1*$^{-/-}$ mice cultured in neural or acidic medium at 7 days, n = 3. Scale bars, 50μm. (C) PAC-mediated currents in single cells (osteoclast precursor) or fused cells (mature osteoclasts) cultured in osteoclastic medium for 3 days, n ≥ 7. (D) PAC-mediated currents in the cells cultured in osteoclastic medium for 3 or 5 days, n ≥ 7. (E, G) TRAP staining for cells isolated from *Pacc1*$^{+/+}$ or *Pacc1*$^{-/-}$ mice cultured in neural or acidic medium at 3 and 5 days, n = 3. Scale bars, 50μm. (F, H) Phalloidin staining

for cells isolated from *Pacc1*$^{+/+}$ or *Pacc1*$^{-/-}$ mice cultured in neural or acidic medium at 3 and 5 days, n = 3. Scale bars, 50μm.

(B, G, H) *$p < 0.05$ compared with the cells isolated from *Pacc1*$^{+/+}$ mice cultured in the neutral medium; and # $p < 0.05$ compared with the cells isolated from *Pacc1*$^{+/+}$ mice cultured in the acidic medium. (C) *$p < 0.05$ compared with the single cell. (D) *$p < 0.05$ compared with Day 3.

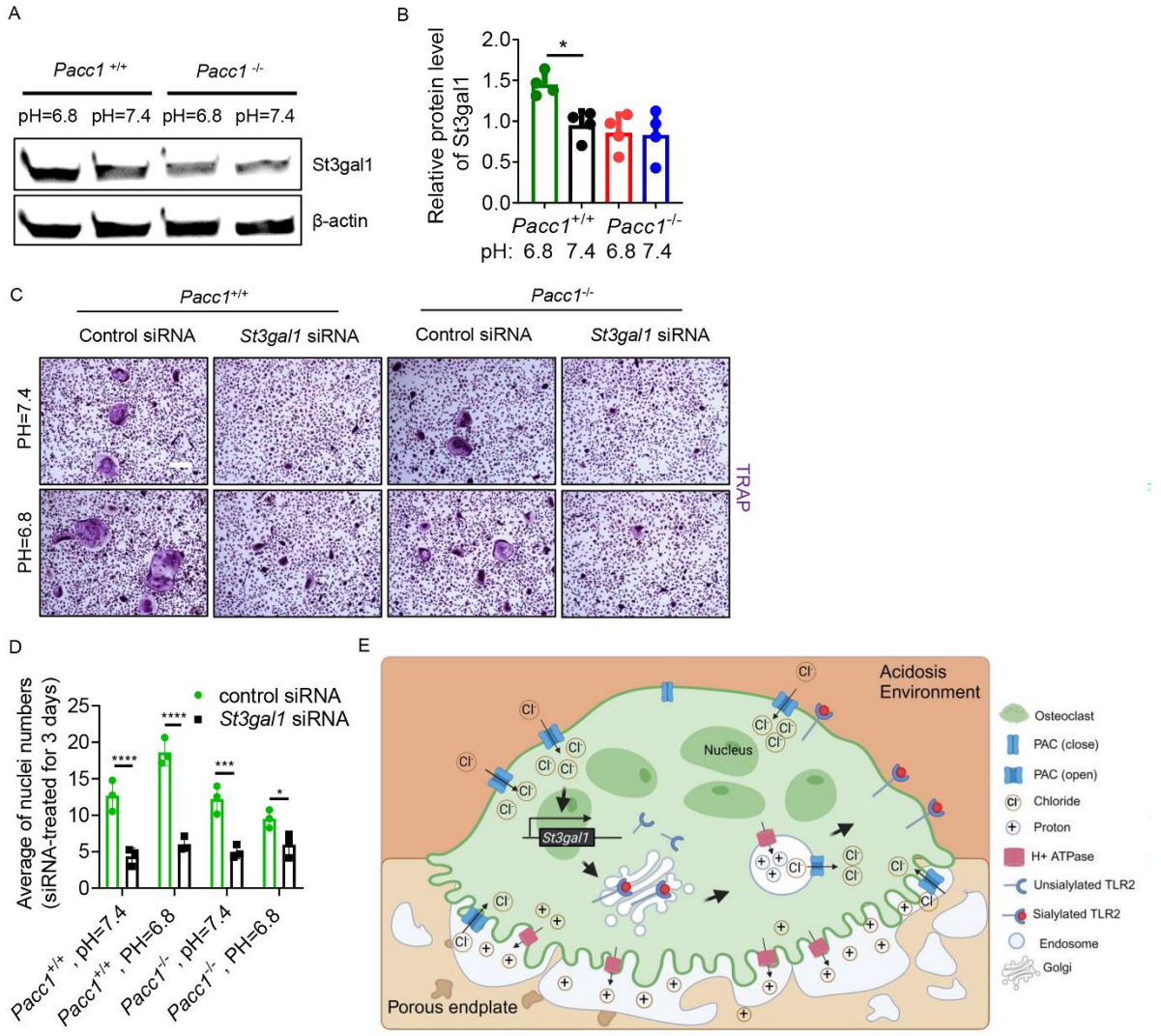

Figure 7. PAC mediates osteoclast fusion through sialyltransferase St3gal1 induced sialylation of TLR2

(A) The representative image and quantitative analysis of Western Blot for St3gal1 protein expression relative to β -action in BMM isolated from *Pacc1*$^{+/+}$, *Pacc1*$^{-/-}$ mice, at pH 6.8 or pH 7.4. (B) Statistic analysis of St3gal1 protein expression in each group, relative to the

Pacc1$^{+/+}$ pH 7.4 group, n = 4. (C, D) TRAP staining for cells isolated from *Pacc1*$^{+/+}$, *Pacc1*$^{-/-}$ mice cultured in neural or acidic medium for 3 days with RANKL stimulation, and control or *St3gal1* siRNA interference, n = 3. Scale bars, 50μm. (E) Acidosis environment in the LSI model could acidify the pH level of intracellular in osteoclast through a synergetic function of PAC on the membrane. The translational expression of *St3gal1* is regulated by PAC at the low pH condition. PAC on the membrane of endosome is responsible for maintaining the post-translational sialylation of TLR2, which mediated by St3gal1 for osteoclast fusion. (B, D) *$p < 0.05$, ***$p < 0.005$, ****$p < 0.001$.

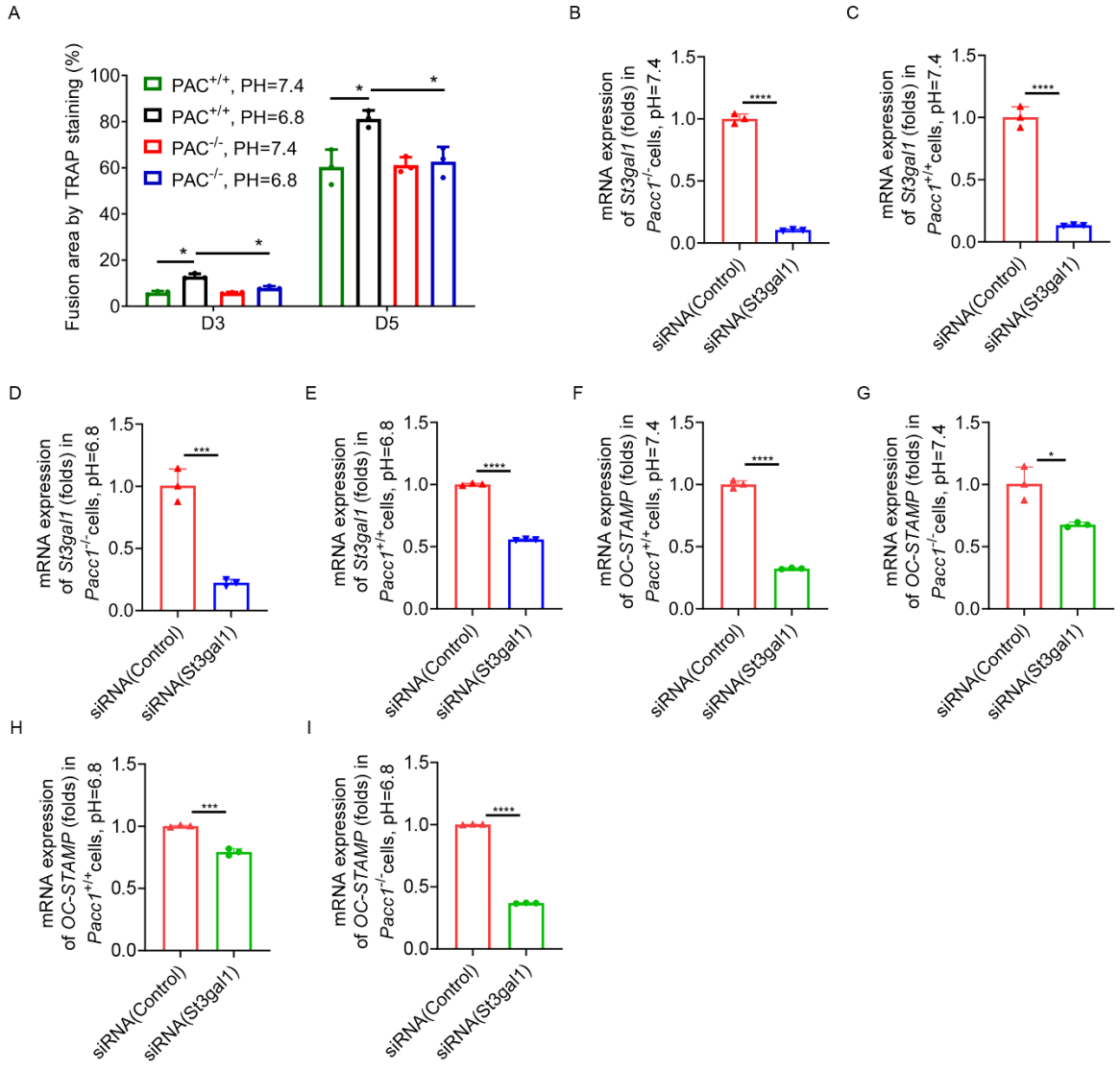

Supplemental Figure 1. RT-PCR analysis of the expression of osteoclast fusion related gene.

787 (A) Quantitative analysis of TRAP staining by fusion area for cells isolated from *Pacc1*$^{+/+}$ or
788 *Pacc1*$^{-/-}$ mice cultured in neural or acidic medium at day 3 and day 5. (B-E) The quantitative
789 analysis of the gene expression of *St3gal1* in *St3gal1* siRNA treated osteoclasts compared to
790 control siRNA treated in *Pacc1*$^{-/-}$ pH 7.4 (B), *Pacc1*$^{+/+}$ pH 7.4 (C), *Pacc1*$^{-/-}$ pH 6.8 (D), *Pacc1*$^{+/+}$
791 pH 6.8 (E). (F-I) The quantitative analysis of the gene expression of *OC-STAMP* in *St3gal1*
792 siRNA treated osteoclasts compared to control siRNA treated in *Pacc1*$^{+/+}$ pH 7.4 (F), *Pacc1*$^{-/-}$
793 pH 7.4 (G), *Pacc1*$^{+/+}$ pH 6.8 (H), *Pacc1*$^{-/-}$ pH 6.8 (I), **p* < 0.05, ****p* < 0.005, *****p* < 0.001.
794

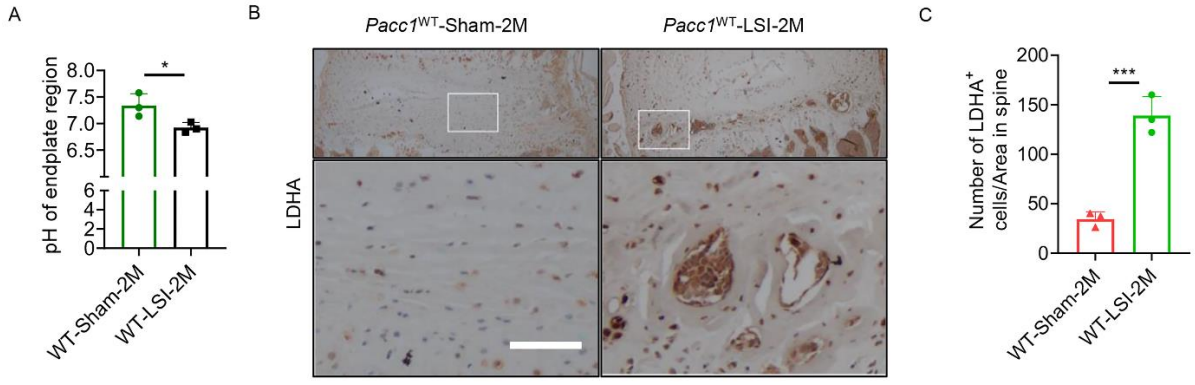

795

796 **Supplemental Figure 2. IHC staining of LDHA in spine tissue section.**

797 (A) The quantitative results of the average pH value at L3-L5 endplates in WT sham or LSI
798 mice. (B) The representative images of IHC staining of LDHA in the spine section in *Pacc1*^{WT}
799 mice with sham or LSI surgery for two months. Scale bar: 0.5 mm. (C) The quantitative analysis
800 of the number of LDHA positive cells per area, **p* < 0.05, ****p* < 0.005.
801